16th World Conference on Earthquake, 16WCEE 2017
Santiago Chile, January 9th to 13th 2017
Paper N° 1060
Registration Code: S-G1462941508

# GROUTED SPLICE SLEEVE CONNECTIONS FOR PRECAST BRIDGE SUBSTRUCTURES IN SEISMIC REGIONS

M. J. Ameli[(1)], C. P. Pantelides[(2)], J. E. Parks[(3)], D. N. Brown[(4)]

[(1)] *Graduate Engineer, Diagnostics, Walter P Moore, mameli@walterpmoore.com*
[(2)] *Professor, Dept. of Civil and Environmental Eng., University of Utah, c.pantelides@utah.edu*
[(3)] *Graduate Research Assistant, Dept. of Civil and Environmental Eng., University of Utah, joel.parks@utah.edu*
[(4)] *Bridge Engineer, Michael Baker International, Madison, WI, dylan.neil.brown@gmail.com*

## Abstract

Connections between precast substructure elements must withstand significant stresses and deformations in earthquakes. Grouted splice sleeve connectors offer good construction tolerances and are considered for prefabricated bridges in seismic regions using accelerated bridge construction. In this research, grouted splice sleeve connectors were used in various configurations to connect half-scale precast bridge columns to footings. The quasi-static cyclic experiments consisted of two precast and one cast-in-place column-to-footing subassemblies. For the first precast specimen the grouted splice sleeve connectors were located in the footing. For the second precast specimen the connectors were placed inside the column end, and reinforcing bars were debonded from concrete in the footing. Experimental results show that a more ductile performance was achieved for the second precast specimen; both precast specimens had an acceptable strength. Computational studies were conducted to simulate the response of each specimen under lateral cyclic loads. Force-based beam-column elements with fiber sections were used to construct the computational model based on plastic hinge weighted integration. The model was validated through both local and global responses with the experiments, and was subsequently used to predict the response of a prototype precast bridge bent under a suite of earthquake induced ground motions.

*Keywords: Accelerated Bridge Construction; Mechanical Coupler; Connections; Cyclic Load Test; Computational Model.*

# 1. Introduction

Recent advances in bridge construction include innovative methodologies that bring about ease of construction and acceleration of the overall project delivery time. Prefabrication of bridge elements contributes to this construction method and facilitates the construction process, whether the bridge is new or a replacement. Connections between such elements in the bridge substructure are critical components in bridges constructed using accelerated bridge construction (ABC). Such connections undergo high levels of earthquake-induced deformations and stresses, while concentrated damage accumulates in localized areas. Strength properties of individual grouted splice sleeve (GSS) connectors were studied previously [1]; tension test results provided information on potential failure modes, ultimate load capacity, and flow of the tensile load. To date, only a few large-scale experimental studies have been conducted utilizing GSS connectors. Aida et al. (2005) and Yoshino et al. (1996) reported on the cyclic performance of large-scale specimens representing a bridge and a building subassembly, respectively [2, 3]. NCHRP report 698 evaluated several connection types applicable to ABC for moderate-to-high seismic regions [4]. The GSS connection was classified as a practical and promising connection type, requiring more research on both strength and deformation properties. In particular, inelastic behavior of such connections under cyclic loads and sensitivity of the response to location of the sleeves were highlighted as issues for further research. Haber et al. (2014) discussed the test results of two half-scale specimens with GSS connectors compared to a cast-in-place control specimen [5]. All specimens exhibited similar performance in terms of ultimate load and energy dissipation; however, the ductility capacity of the precast specimens was an order of magnitude smaller than the control specimen. Tazarv et al. (2014) described an innovative procedure to improve the ductility capacity of columns with GSS connectors embedded in the column [6]. The footing dowel bars were debonded within a pedestal to allow for better spread of plasticity and to postpone bar fracture. Ameli et al. (2015) discussed a series of experiments on precast subassemblies with grouted-fastened connectors placed adjacent to the column-to-cap beam interface; test results showed that a pullout failure occurred for one of the subassemblies [7].

Analytical studies are needed for a more thorough investigation of the overall aspects of the performance. To provide a basis for a better application of the experimental results in actual design and construction, analytical models were developed for precast bridge piers with GSS connectors [6, 8]. These analytical models were successful in reproducing the corresponding experimental results.

As part of an extensive research program at the University of Utah, three half-scale specimens were tested under quasi-static cyclic displacements. Two precast column-to-footing specimens incorporated one type of GSS connector for which the bars were grouted at both ends. The third specimen was built monolithically to serve as the control. The experimental program is presented; furthermore, computational models were developed and validated with the experiments to simulate the response of prototype precast bridge bents to earthquake induced ground motions.

# 2. Experiments

Quasi-static cyclic tests were conducted on three half-scale specimens, two of which were joined by means of the GSS connectors shown in Fig. 1. Tensile and compressive force transfer between the two spliced bars occurs by means of bond stresses between bars and high-strength grout inside a cast-iron steel connector. These connectors were incorporated in the footing of specimen Precast-1 while the dowel bars protruded from the column end. The second precast specimen, Precast-2, was composed of a precast column and precast footing connected by GSS connectors which were cast at the column base; the dowel reinforcing bars protruded from the footing. These dowel bars were debonded from the concrete over an 8.0 in. region below the footing surface. The control specimen CIP was constructed monolithically without any GSS connectors.

## 2.1 Design of Half-Scale Specimens

The specimens were designed and detailed to simulate bridges constructed in the State of Utah, following the AASHTO LRFD Bridge Design Specifications, and the AASHTO Guide Specifications for LRFD Seismic Bridge Design [9, 10]. A circular configuration of column longitudinal bars and an octagonal column cross-


Fig. 1 – Grouted splice sleeve (GSS) connector used in this study.

section were adopted to facilitate pre-casting of the columns. Currently, the aforementioned design codes in addition to the Caltrans Seismic Design Criteria (SDC) prohibit splicing of reinforcement, including mechanical anchorage devices, in the plastic hinge region of ductile members, for bridges located in moderate-to-high seismic areas [11]. In the AASHTO Guide Specifications for LRFD Seismic Bridge Design, this would apply to Seismic Design Categories (SDC) C and D. Thus, the preliminary design was developed for CIP, which was then adjusted to accommodate the GSS connectors within the precast specimens as needed, and essential modifications were considered accordingly.

The specimens were half-scale models of common prototype highway bridges. The column height for all specimens was 8 ft 6 in. with a 21 in. octagonal cross-section. The top 18 in. length of the columns was changed from an octagon to a 21 in. square for testing. Six No. 8 bars in a circular arrangement and a No. 4 spiral with a pitch of 2½ in. made up the column reinforcement. The longitudinal and volumetric transverse reinforcement ratios were 1.3% and 1.9%, respectively. The footing was designed as a 6-ft long x 3-ft wide x 2-ft deep precast concrete element and consisted of No. 8 longitudinal bars enclosed by No. 4 double hoops spaced at 2.5 in. on center. The footing was designed to remain elastic. Shear failure was avoided by using a shear span-to-depth ratio greater than 5.0 with closely spaced transverse reinforcement. The desirable column failure mode was either flexural or splice failure. Fig. 2 shows the details and configuration of the three specimens discussed in this paper.

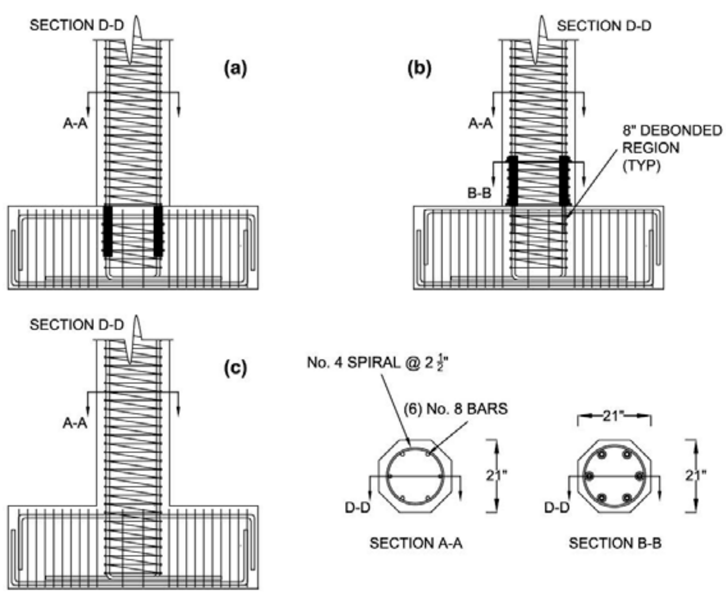


Fig. 2 – Details of test subassemblies: (a) Precast-1; (b) Precast-2; (c) CIP.

## 2.2 Test Setup and Displacement History

The specimens were attached to the test frame using high strength bolts; the lateral cyclic load and axial load were simultaneously applied to the column top. A 120-kip servo-controlled actuator, with an overall stroke of 18 in. applied the lateral cyclic load to the precast specimens; the control specimen was tested using a 250-kip servo-controlled actuator with an overall stroke of 24 in. An axial load of 6% of the column compressive capacity was applied to simulate gravity loads. An actuator placed on top of the column, applied the compression force to a steel spreader beam through two high strength threaded rods, as shown in the test setup of Fig. 3(a). The displacement history consisted of increasing amplitudes of the predicted column yield displacement [12]. Two cycles were employed for each displacement step. Fig. 3(b) shows the drift history. The drift ratio is defined as the lateral displacement of the column top divided by the distance from top of the footing to center of the lateral load, which was 96 in., as shown in Fig. 3(a).

## 2.3 Summary of Test Results

### 2.3.1 Test-day Material Properties

Tension tests of reinforcing bars were conducted along with compression tests of concrete cylinders and grout cubes for each specimen. No. 8 ASTM A706 Grade 60 reinforcement was used as longitudinal column bars which had average yield and ultimate strengths of 68 ksi and 93 ksi, respectively. Table 1 contains the compression test results for the concrete and grout on the day of test.

### 2.3.2 Hysteretic Performance and Observations

The overall response of the three specimens was good as implied by the wide and stable hysteresis loops that indicate a relatively high energy dissipation capacity, as shown in Fig. 4. The damage states mark three major events during the cyclic tests: end of flexural crack formation and initiation of cover spalling, yield penetration, and fracture of column longitudinal reinforcing bars.

Specimen Precast-1 had a stable performance up to the first cycle of the 7% drift ratio, during which the column east reinforcing bar fractured at a section 2 in. above the column-to-footing interface, due to low-cycle fatigue. There was no sign of excessive in-cycle or cyclic strength deterioration before fracture of the extreme east reinforcing bar. The test was terminated after completion of the 7% drift ratio as a result of a 35% strength reduction. The displacement ductility of this specimen was found to be 6.1; this quantity was calculated using the average cyclic envelope of the force-displacement response and widely accepted procedures based on the concept of equal energy of an idealized elasto-plastic system [13].

The overall hysteretic response of specimen Precast-2 indicated an entirely satisfactory and ductile performance. The hysteresis loops of this specimen were wide and stable with minimal strength deterioration up to the first cycle during the 8% drift ratio, when the extreme east column reinforcing bar fractured ½ in. below the column-to-footing interface. Deboning of dowel bars inside the footing of this precast specimen resulted in an extended performance life, compared to Precast-1. The displacement ductility of this specimen was found to

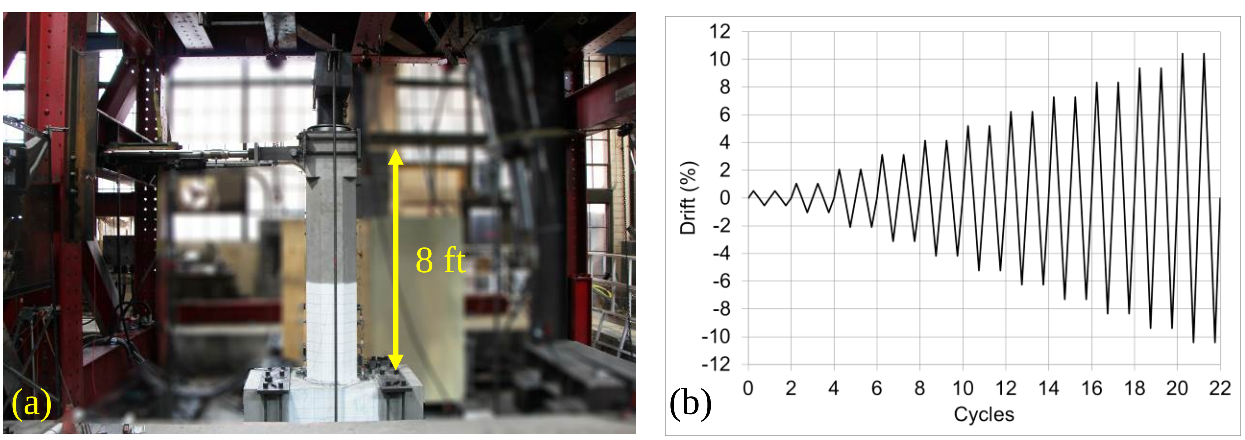


Fig. 3 – (a) Test setup; (b) Drift history.

Table 1 – Test-day compressive strength of concrete and grout (ksi).

| Specimen | Concrete | Grout |
|---|---|---|
| Precast-1 | 5.5 | 13.5 |
| Precast-2 | 8.4 | 14.6 |
| CIP | 6.7 | NA |

be 6.8 implying that a more ductile response was achieved when GSS connectors were in the column and bars were debonded in the footing.

Control specimen CIP had stable hysteresis loops with slight strength degradation caused by spalling of the relatively large unconfined concrete cover. To keep the sectional configuration of column reinforcing bars identical among all specimens, specimen CIP had the thickest cover so that the location of the column longitudinal bars remained unchanged. As expected, specimen CIP had the longest performance life compared to the two precast specimens. For this specimen, the extreme west column reinforcing bar fractured towards the end of the second cycle of the 8% drift ratio, at a section 1 ½ in. above the column-to-footing interface. Subsequently, the extreme east column reinforcing bar fractured during the first cycle of the 9% drift ratio, 2 in. above the interface achieving a displacement ductility of 8.9. More detailed discussion on the experimental results can be found elsewhere [14].

## 3. Computational Study

### 3.1 Description of Proposed Modeling Strategy

The objective of the computational study was to develop a predictive modeling strategy for simulation of precast concrete bridge substructures with GSS connections. The proposed computational models were validated with the experiments using both global and local response comparisons. The models were composed of a force-based

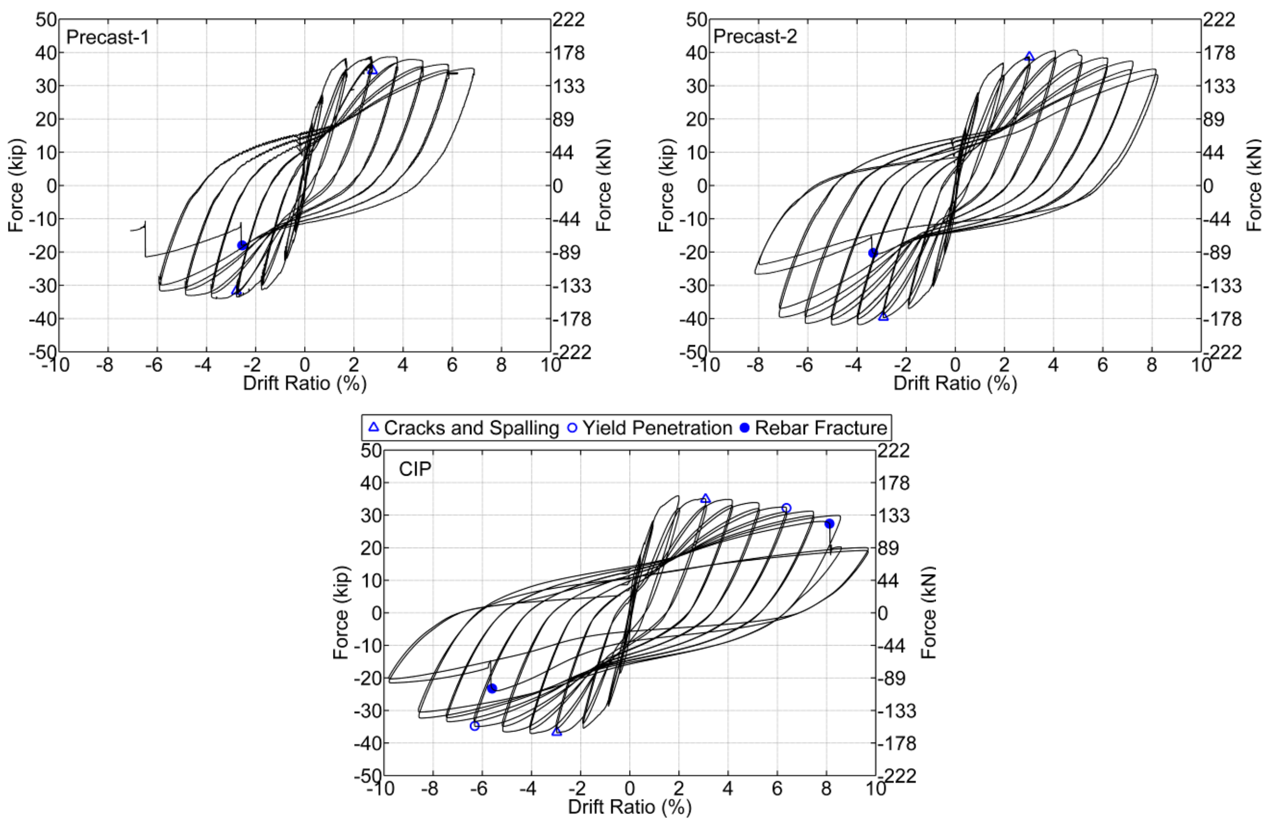


Fig. 4 – Force-drift response of subassemblies.

beam-column element with distributed plasticity or fiber models including cross-sections that were discretized into a finite number of fibers; pertinent uniaxial material stress-strain relationships were assigned to each type of fiber. Numerical integration was evaluated along the element to obtain the global response.

To prevent the loss of objectivity which was observed when using the force-based element for the subassemblies studied herein, the plastic hinge integration scheme of Scott and Fenves (2006) was adopted in this study so that the proposed model could be used for a wide range of reinforced or precast concrete components [15]. A user-defined analytical plastic hinge length is used with this particular beam-column element. In the absence of an empirical relationship for estimating the plastic hinge length for precast components with GSS connections, an iterative procedure was adopted to obtain this quantity. The iteration was continued until the difference between the response of the model and experiment was less than 12%. Column lateral strength capacity and base curvature were used for global and local response comparisons, respectively.

The proposed model was composed of two nodes and one beam-column element as shown in Fig. 5, using the OpenSees framework [16, 17]. Mander's model was used to model the unconfined concrete cover and the confined concrete core [18]. The octagonal cross-section was approximated by a circle of an equal cross-sectional area for ease of discretization. Column reinforcing bars were modeled using ReinforcingSteel material which is capable of tracking the strain history and determining the low-cycle fatigue life of the bars [19]; this capability was used in the validation process to find the termination point in the simulations. To account for the softening effects of bond-slip, reinforcing bars with a pseudo stress-strain relationship were used in the plastic hinge zone of the columns. Following the iterative process, a plastic hinge length equal to 8 in., 10 in., and 12 in. was determined for specimens Precast-1, Precast-2, and CIP, respectively; the value obtained for CIP correlates well with the empirical relationship from Panagiotakos and Fardis (2001) [20].

## 3.2 Validation of Computational Models

The hysteresis response of the three specimens is shown in Fig. 6(a), up to the last completed drift ratio, including both the experimental results and the results from the proposed computational models. The proposed models correctly identified the cycle and drift ratio within which bar fracture occurred. The results from the proposed models are in a close agreement with the experiments. The absolute difference between the peak lateral force of the experiment and the model was 6%, 1%, and 5% for CIP, Precast-1, and Precast-2, respectively.

The moment-curvature envelope for the push direction of each specimen is presented in Fig. 6(b), up to the end of the 6% drift ratio, when instrumentation devices were removed from the specimens. The curvature values are normalized by multiplying the average curvature by the column thickness which was 21 in. The corresponding computational results suggest that the proposed model is capable of replicating the sectional

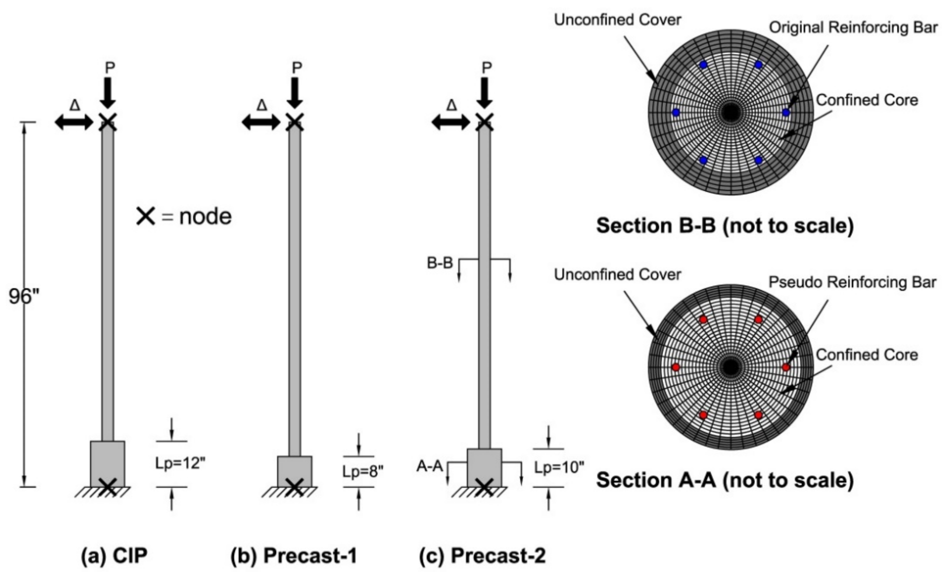


Fig. 5 – Computational model layout.

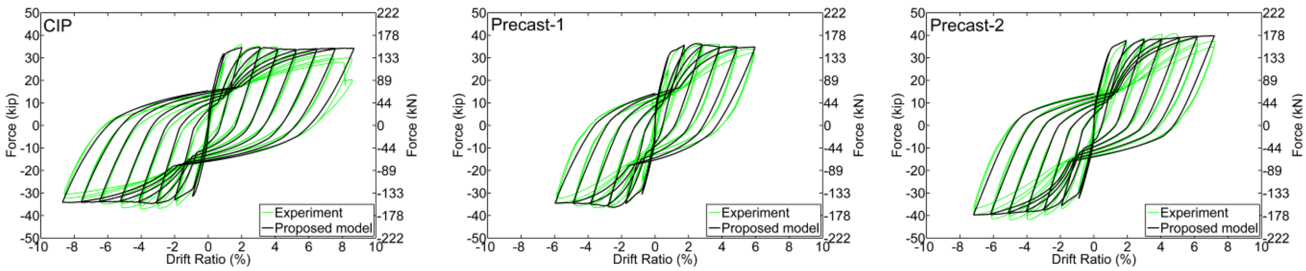


(a)

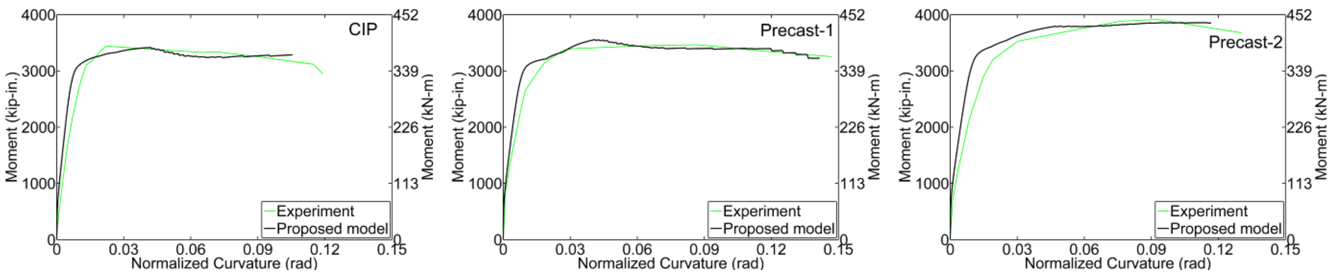


(b)

Fig. 6 – Comparison between experiment and computational models: (a) Global response; (b) Local response.

response in addition to the global response. At 6% drift ratio, there is an 11%, 4%, and 11% difference between the peak curvature capacity obtained from the experiments and that of the analyses for CIP, Precast-1, and Precast-2, respectively.

## 4. Parametric Study

A parametric study was developed, using 32 column models, to investigate the response sensitivity of the proposed model to potential changes in pertinent modeling parameters. A 3-ft circular column reinforced with No. 9 longitudinal bars was used to simulate the response of a cast-in-place and a precast column with details similar to CIP and Precast-2, respectively. Two levels of longitudinal bar reinforcement ratio were selected considering practical aspects of the design, that is, 1.38% and 1.96% corresponding to 14 No. 9 and 20 No. 9 bars, respectively. Two column aspect ratios equal to 4.0 and 5.0 were included indicating a column height of 12 ft and 15 ft, respectively. Two axial load levels were employed with an axial load index (ALI) equal to 5% and 10%; and lastly, design displacement ductility values equal to 7.0 and 11.0 were considered to study different transverse reinforcement alternatives.

Fig. 7 shows the details for four CIP and four Precast-2 models with a height equal to 12 ft and reinforced with 14 No. 9 longitudinal bars (the 24 other cases are not shown for brevity). A plastic hinge length equal to 17.28 in. was obtained for the CIP column model in this category, using the empirical relationship found in Panagiotakos and Fardis (2001) [20]. For the precast alternatives with Precast-2 model details in this category, a reduced plastic hinge length was incorporated using a reduction factor of 5/6 which was determined for the validated computational models, as discussed in the previous section; thus, the plastic hinge length for the precast alternatives in this category was 14.40 in.

Sample analysis results are presented in Fig. 8 for a column model with details similar to CIP and a column model with details similar to Precast-2. Fig. 8(a) shows that the core concrete crushed barely after fracture of the extreme east column reinforcing bar for the CIP model; hence the failure mode was bar fracture due to low-cycle fatigue. On the other hand, Fig. 8(b) shows that the Precast-2 model failed due to crushing of the core concrete near the peak displacement of the first cycle during the 6% drift ratio. The ultimate displacement for the CIP model was 8.64 in., corresponding to a 6% drift ratio, while it was 7.65 in. (or 5.3% drift ratio) for the Precast-2 model; this indicates a reduction in displacement capacity for the precast alternative which can be seen in Fig. 8(c) that shows the cyclic envelopes of the hysteresis responses. Strain variation in the

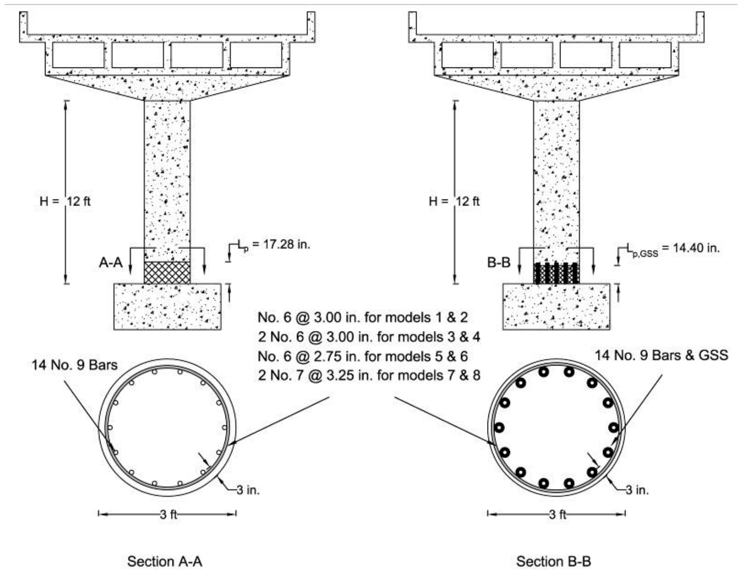


Fig. 7 – Model details for 8 columns with a height equal to 12 ft and 14 No. 9 longitudinal bars.

extreme longitudinal bar, shown in Fig. 8(d), implies that a larger sectional demand was introduced to the column end of the Precast-2 model which resulted in premature fracture of column bars.

Fig. 9(a) shows the cyclic envelopes for all CIP models reinforced with 14 No. 9 longitudinal bars. The overall response of the columns follows a logical trend which is expected to occur for reinforced concrete members under simultaneous lateral and axial loading. For instance, the strength capacity of the columns

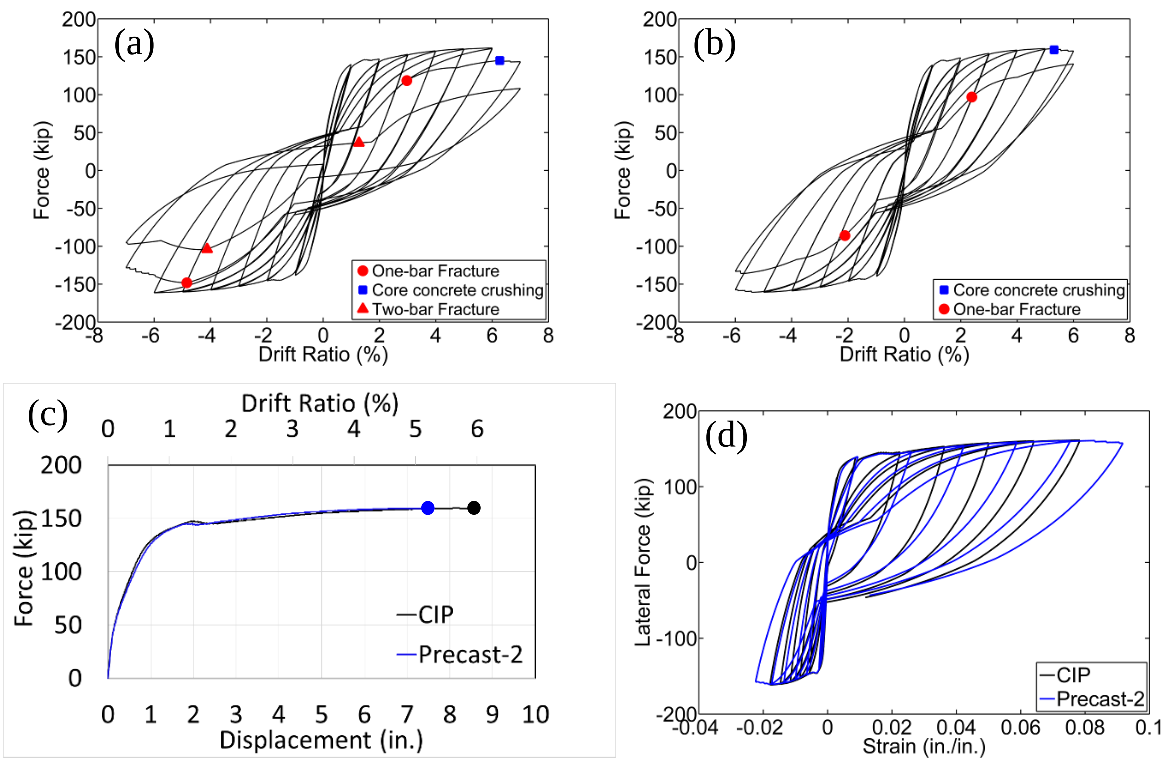


Fig. 8 – Example of analysis response comparison for 12-ft high CIP and Precast-2 models with 14 No. 9 bars, 10% ALI, and design displacement ductility of 7.0: (a) Hysteresis response of CIP model; (b) Hysteresis response of Precast-2 model; (c) Cyclic envelope for both column models; (d) Strains in the column extreme reinforcing bar for two models.

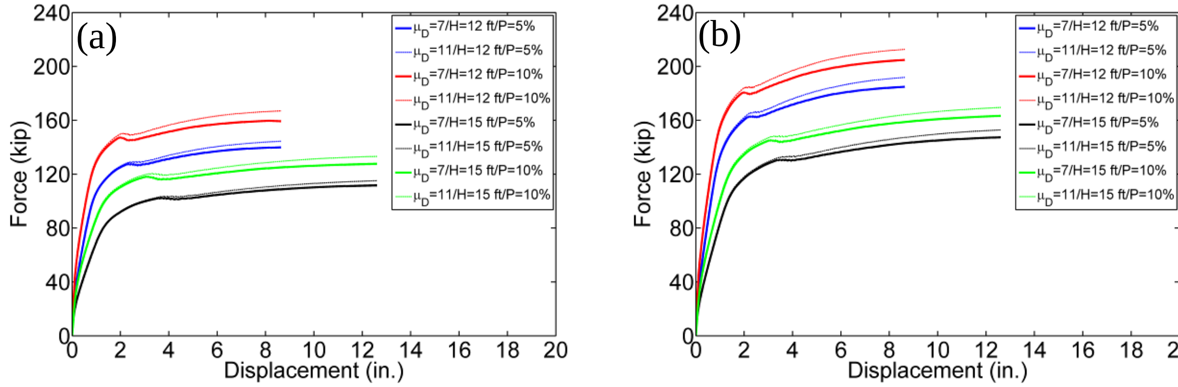


Fig. 9 – Comparison of global response for CIP models under varying parameters: (a) Column models reinforced with 14 No. 9 bars; (b) Column models reinforced with 20 No. 9 bars.

increased with an increase in axial load, whereas the strength decreased with an increase in column height. Similarly, columns with 20 No.9 longitudinal bars had an expected performance under varied parameters. Fig. 9(b) shows the cyclic envelopes for all eight CIP model alternatives with 20 No. 9 longitudinal bars. It is important to note that the effects of parameter variation are only presented using CIP columns for brevity.

## 5. Prototype Precast Bridge Bents with GSS Connections

The proposed model which was validated with the experiments and later verified using a parametric study was used to model one monolithic and two precast bridge bents with similar details to Precast-1 and Precast-2 specimens. Two types of analysis were performed: (1) static cyclic analysis to find the capacity of the systems, and (2) nonlinear time-history analysis to find the level of demand on the bridge bents. Fig. 10 presents the bridge bent system for the three bent alternative models.

The computational model of the bridge bents was composed of 11 nodes and 10 elements, as shown in Fig. 11. The cap beam was modeled using an elastic element called elasticBeamColumn in the OpenSees

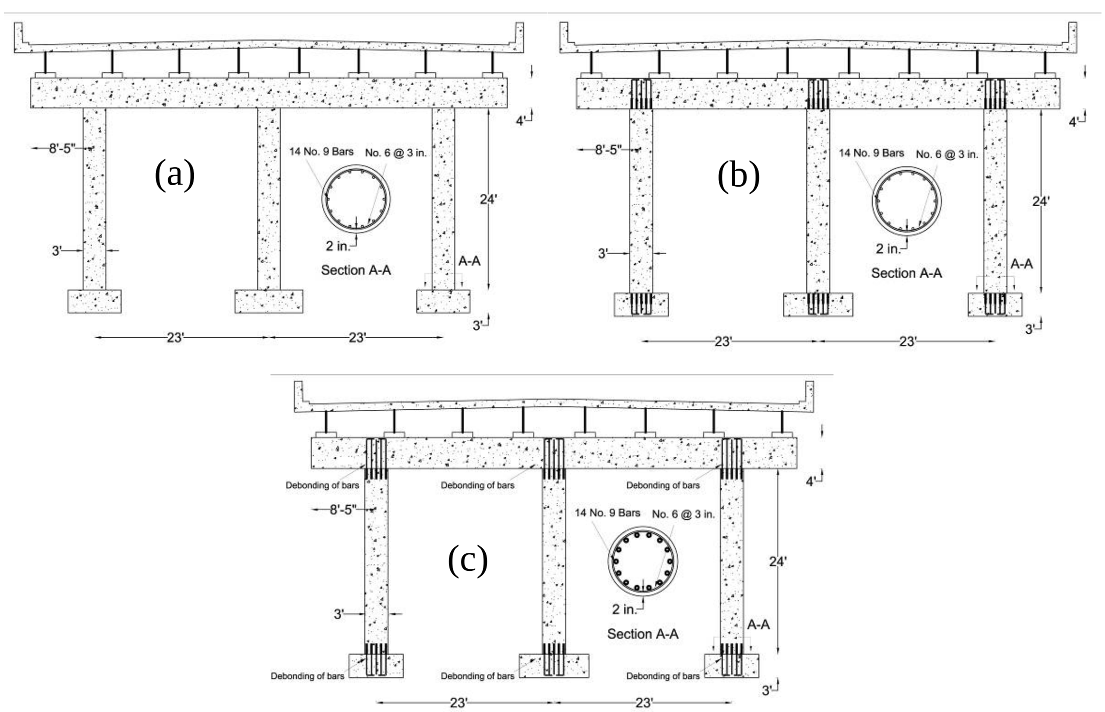


Fig. 10 – Bridge bent alternatives: (a) CIP bent; (b) Precast-1 bent; (c) Precast-2 bent.

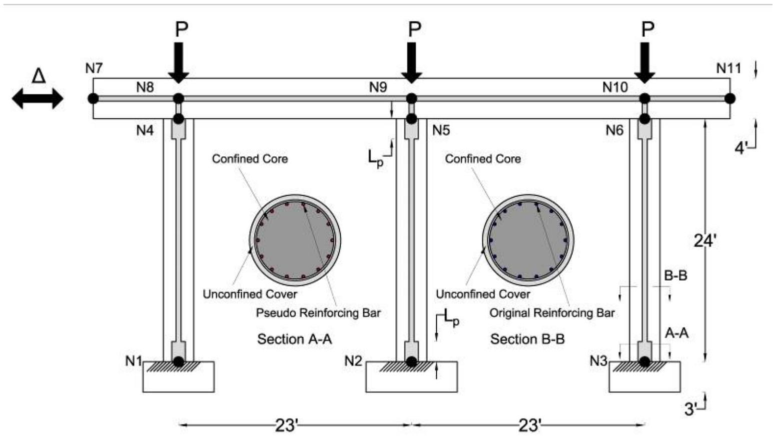


Fig. 11 - Computational model layout for bridge bent system.

element library. This implies that plastic hinging could only occur in the columns, therefore the columns were modeled using forceBeamColumn elements with a plastic hinge integration scheme [15]. Elastic elements with rigid links (rigidLink) were incorporated at the upper end of the ductile columns inside the cap beam to constrain the rotational and translational degrees of freedom. P-Δ effects were included in the cyclic analysis to consider the effects of geometric nonlinearity.

The static cyclic analysis revealed that the strength of the three bent systems was comparable, whereas the displacement capacity of the precast bents was smaller than that of the CIP bent. The CIP bent had a failure mode of bar fracture at 6% drift ratio, while bents Precast-1 and Precast-2 failed due to crushing of the core concrete at a 4.6% and 5.5% drift ratio, respectively.

A suite of earthquake induced ground motions was selected based on the guidelines found in the AASHTO Guide Specifications [10]. It was assumed that the bridge was located in downtown Salt Lake City in the Utah which is considered as a seismic design category (SDC) D, since the one-second period design spectral acceleration ($S_{D1}$) exceeds 0.5 g. Overall, eight ground motions were selected from the PEER Ground Motion Database, representing the seismic characteristics of the bridge location in terms of earthquake magnitude, faulting mechanism, proximity to fault rupture, and site class condition [21].

Fig. 12 presents the drift demands for all bridge bents under the eight ground motions considered in this study; it also includes the drift capacity of each bent using horizontal lines in respective colors. Fig. 12 shows that the largest drift maximum demand was 1.97% for bent CIP, whereas the maximum drift demand for bent

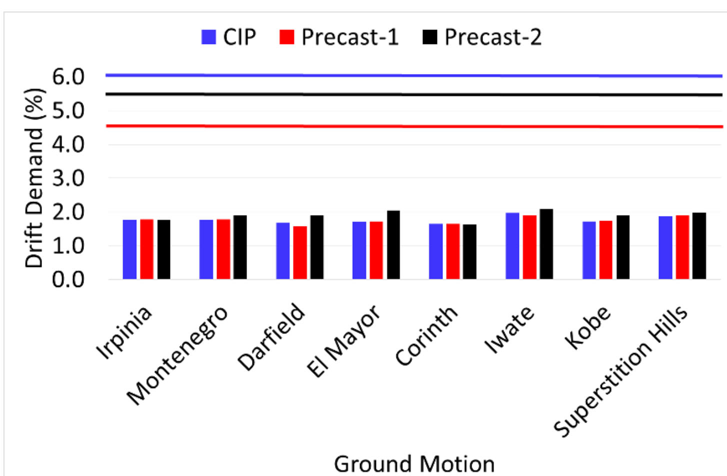


Fig. 12 – Comparison of bridge bent drift demands under a suite of ground motions; horizontal lines shows drift capacity for the bridge bents.

Precast-1 and bent Precast-2 was equal to 1.90% and 2.07%, respectively. Compared to the drift capacity of the three bridge bents, there was a considerable reserve capacity for the three systems. Furthermore, it was noted that Precast-2 had a slightly increased drift demand under all ground motions except Irpinia and Corinth; this is attributed to the debonding effects of the dowel bars on the overall stiffness of the precast bridge bent.

## 6. Conclusions

The experimental investigation on half-scale bridge column-to-footing subassemblies, in addition to the computational study provided valuable information on the performance of precast bridge column connections using grouted splice sleeve connectors. A summary of conclusions follows:

- The experiments showed that the control specimen CIP and the precast specimens Precast-1 and Precast-2 had wide and stable hysteresis loops implying a high and comparable energy dissipation capacity for the three subassemblies.
- The strength of the tested subassemblies was comparable, while there was a distinct reduction in the displacement capacity of the precast subassemblies. Specimen CIP failed due to low-cycle fatigue bar fracture during the 2$^{nd}$ cycle of the 8% drift ratio. Precast-1 and Precast-2 specimens failed prematurely due to low-cycle fatigue bar fracture during the 1$^{st}$ cycle of the 7% drift ratio and 1$^{st}$ cycle of the 8% drift ratio, respectively.
- The computational study included an iterative procedure to validate the proposed modeling strategy with the experiments, and resulted in determining the plastic hinge length for the three tested subassemblies in the absence of empirical relationships for precast columns with grouted splice sleeve connectors. The obtained plastic hinge length for specimen CIP which was found to be 12.0 in. was in good agreement with an empirical relationship for monolithically constructed columns. A reduced plastic hinge length equal to 8.0 in and 10.0 in. was obtained for specimens Precast-1 and Precast-2, respectively.
- The absolute error between the strength capacity of the validated models and that of the tested subassemblies was between 1% and 5% (global response validation). The absolute error for the column base curvature capacity of the subassemblies was between 4% and 11% (local response validation).
- The parametric study using actual size bridge columns with varying parameters verified that the response of the computational model was in good agreement with the anticipated performance of reinforced concrete columns using available analytical methods. It was observed that the strength capacity of the simulated column increased with an increase in axial load, design target ductility, or longitudinal reinforcement ratio; the strength capacity of the simulated column decreased with an increase in the height of the column.
- The parametric study revealed that the proposed model was capable of capturing the reduced displacement capacity of the precast columns as a result of an increased sectional demand.
- Three prototype bridge bents modeled using the proposed modeling strategy had a comparable strength capacity but different displacement capacity, as shown by the results of static cyclic analysis. A drift capacity of 6%, 4.6%, and 5.5% was obtained for bridge bent systems CIP, Precast-1, and Precast-2, respectively.
- Nonlinear time-history analyses on the prototype bridge bents, using a suite of scaled earthquake induced ground motions, showed that drift demands were considerably lower than the drift capacities for the three simulated bridge bent systems. The maximum drift demand was 1.97%, 1.90%, and 2.07% for bent systems CIP, Precast-1, and Precast-2, respectively.

## 7. Acknowledgements

The authors would like to acknowledge the financial support of the Utah, New York State, and Texas Departments of Transportation, the Mountain-Plains Consortium, and the Graduate School of the University of Utah. The authors wish to thank Dr. Lawrence D. Reaveley and Mark Bryant of the University of Utah for their invaluable input throughout the experimental study. The authors are also grateful for the donation of materials by

Splice Sleeve North America, and the assistance of Hanson Structural Precast (Forterra).

## 8. References

[1] Jansson, P. O. (2008): Evaluation of Grout-Filled Mechanical Splices for Precast Concrete Construction. *Report R-1512*, Michigan Department of Transportation, Lansing, MI.

[2] Aida, H., Tanimura, y., Tadokoro, T., and Takimoto, K. (2005): Cyclic Loading Experiment of Precast Columns of Railway Rigid-Frame Viaduct Installed with NMB Splice Sleeves. *Proceedings of the Japan Concrete Institute*, 27 (2).

[3] Yoshino, T., Kobayashi, K., and Ase, M. (1996): Intensive Shear Reinforcing Method for PCA Members with Splice Sleeve Joint. *Proceedings of the 11th World Conference on Earthquake Engineering*, Acapulco, Mexico.

[4] Marsh, M. L., Wernly, M., Garett, B. E., Stanton, J. F., Eberhard, M. O., and Weinert M. D. (2011): Application of Accelerated Bridge Construction Connections in Moderate-to-High Seismic Regions. *NCHRP Report 698*, National Cooperative Highway Research Program, Washington, DC.

[5] Haber, Z. B., Saiidi, M. S., and Sanders, D. H. (2014): Seismic Performance of Precast Columns with Mechanically Spliced Column-Footing Connections. *ACI Struct. J.*, 111 (3), 639-650.

[6] Tazarv, M., and Saiidi, M. S. (2014): Next Generation of Bridge Columns for Accelerated Bridge Construction in High Seismic Zones. *Rep. No. CCEER 14-06*, Center for Civil Engineering Earthquake Research, Dept. of Civil and Environmental Engineering, Univ. of Nevada, Reno, NV.

[7] Ameli, M. J., Parks, J. E., Brown D. N., and Pantelides, C. P. (2015): Seismic Evaluation of Grouted Splice Sleeve Connections for Reinforced Precast Concrete Column-to-Cap beam Joints in Accelerated Bridge Construction. *PCI Journal*, 60 (2), 80-103.

[8] Haber, Z. B., Saiidi, M. S., and Sanders, D. H. (2015): Behavior and Simplified Modeling of Mechanical Reinforcing Bar Splices. *ACI Struct. J.*, 112 (2), 179-188.

[9] AASHTO. (2012): *AASHTO LRFD bridge design specification*, Washington, DC.

[10] AASHTO. (2011): *AASHTO guide specifications for LRFD seismic bridge design*, Washington, DC.

[11] Caltrans. (2010): *Seismic design criteria (SDC)*, version 1.6, Sacramento, CA.

[12] American Concrete Institute (ACI). (2013): *Guide for Testing Reinforced Concrete Structural Elements Under Slowly Applied Simulated Seismic Loads*. ACI 374, Farmington Hills, MI.

[13] Park, R. (1989): Evaluation of Ductility of Structures and Structural Assemblages from Laboratory Testing. *Bulletin of the New Zealand National Society for Earthquake Engineering*, 22 (3), 155-166.

[14] Pantelides, C.P., Ameli, M. J., Parks, J.E., and Brown, D.N. (2014): Seismic Evaluation of Grouted Splice Sleeve Connections for Precast RC Bridge Piers in ABC. *Rep. No. UT-14.09*, Utah Department of Transportation Research Division, SLC, UT.

[15] Scott, M. and Fenves, G. (2006): Plastic Hinge Integration Methods for Force-Based Beam–Column Elements. *J. Struct. Eng.*, 10.1061/(ASCE)0733-9445(2006)132:2(244), 244-252.

[16] McKenna, F., Fenves, G., and Scott, M. (2000): Open System for Earthquake Engineering Simulation (OpenSees). Univ. of California, Berkeley, CA. (http://opensees.berkeley.edu)

[17] McKenna, F., Scott, M., and Fenves, G. (2010): Nonlinear Finite-Element Analysis Software Architecture Using Object Composition. *J. Comput. Civ. Eng.*, 10.1061/(ASCE)CP.1943-5487.0000002, 95-107.

[18] Mander, J. B., Priestley, M. J. N., and Park, R. (1988): Theoretical Stress-Strain Model for Confined Concrete. *J. Struct. Eng.*, 10.1061/(ASCE)0733-9445(1988)114:8(1804), 1804-1826.

[19] Kunnath, S., Heo, Y., and Mohle, J. (2009): Nonlinear Uniaxial Material Model for Reinforcing Steel Bars. *J. Struct. Eng.*, 10.1061/(ASCE)0733-9445(2009)135:4(335), 335-343.

[20] Panagiotakos, T. B., and Fardis, M. N. (2001): Deformations of Reinforced Concrete Members at Yielding and Ultimate. *ACI Struct. J.*, 98 (2), 135-148.

[21] Pacific Earthquake Engineering Research Center (PEER): *PEER Strong Motion Database*. ⟨http://ngawest2.berkeley.edu/⟩ (Feb., 2016).